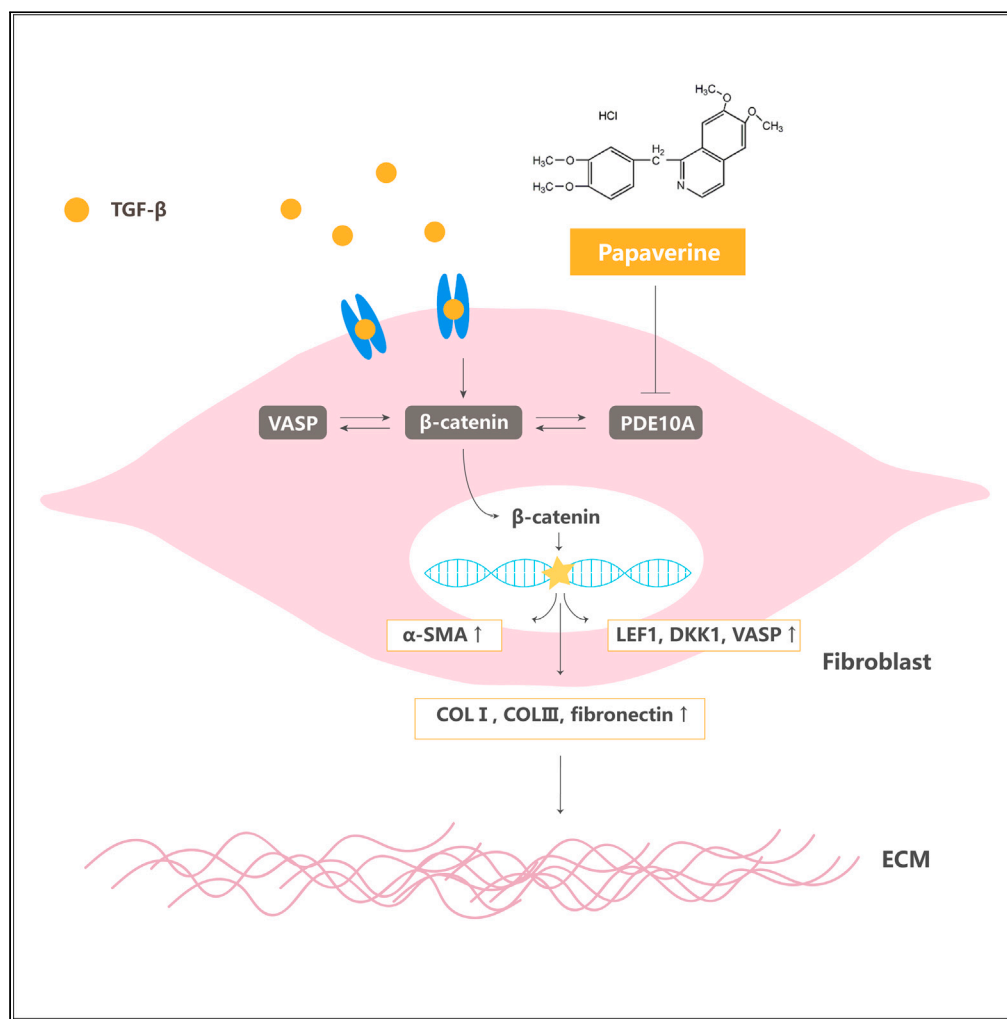


## Article

## Phosphodiesterase type 10A inhibitor attenuates lung fibrosis by targeting myofibroblast activation



Ya-Jun Li, Jian-Rong Shi, Shu-Chan Li, ..., Xin-Wei Cao, Zi-Gang Li, Hui-Fang Tang

tanghui.fang@zju.edu.cn

**Highlights**

PDE10A inhibitor targeting inhibit myofibroblast differentiation and lung fibrosis

Papaverine and pirfenidone share similar anti-fibrotic and anti-oxidant effects

β-catenin/VASP pathway mediated the anti-fibrotic effect of papaverine

VASP may be used as a novel marker for lung fibrosis

## Article

## Phosphodiesterase type 10A inhibitor attenuates lung fibrosis by targeting myofibroblast activation

Ya-Jun Li,<sup>1,6</sup> Jian-Rong Shi,<sup>2,6</sup> Shu-Chan Li,<sup>1</sup> Lu-Ming Wang,<sup>3</sup> Rana Dhar,<sup>1</sup> Ning Li,<sup>1</sup> Xin-Wei Cao,<sup>1</sup> Zi-Gang Li,<sup>4</sup> and Hui-Fang Tang<sup>1,5,7,\*</sup>

## SUMMARY

**Pulmonary fibrosis (PF) is a fatal and irreversible respiratory disease accompanied by excessive fibroblast activation. Previous studies have suggested that cAMP signaling pathway and cGMP-PKG signaling pathway are continuously down-regulated in lung fibrosis, whereas PDE10A has a specifically expression in fibroblasts/myofibroblasts in lung fibrosis. In this study, we demonstrated that over-expression of PDE10A induces myofibroblast differentiation, and papaverine, as a PDE10A inhibitor used for vasodilation, inhibits myofibroblast differentiation in human fibroblasts. Meanwhile, papaverine alleviated bleomycin-induced pulmonary fibrosis and amiodarone-induced oxidative stress, papaverine down-regulated VASP/ $\beta$ -catenin pathway to reduce the myofibroblast differentiation. Our results first demonstrated that papaverine inhibits TGF $\beta$ 1-induced myofibroblast differentiation and lung fibrosis by VASP/ $\beta$ -catenin pathway.**

## INTRODUCTION

Pulmonary fibrosis (PF) is a chronic, aggressive and lethal lung disease with pathological deposition of connective tissue, repetitive injury to the alveolar wall, the abnormal accumulation of fibroblasts/myofibroblasts, excessive deposition of extracellular matrix (ECM) components, and abnormal tissue repair lead to loss of lung function.<sup>1</sup> After prognosis for PF, a 5 years survival rate of patients is 48%.<sup>2</sup> Despite extensive research efforts over the last few decades, only two drugs, pirfenidone and nintedanib, are currently available to retard the decline in lung function.<sup>3</sup> Thus, it is important to clarify the mechanism to suppress this disease.

Idiopathic pulmonary fibrosis (IPF) is a most common progressive interstitial lung disease (ILD). The major player in the process of lung stiffening is the myofibroblast, characterized by the presence of alpha-smooth muscle actin ( $\alpha$ -SMA), which accumulate excess ECM components, such as fibronectin (FN), collagen I (Col I) and collagen III (Col III).<sup>4</sup> Meanwhile, myofibroblasts failed to disappear after normal wound healing and presented resistance to apoptosis, as exemplified by human IPF.<sup>5</sup> Transforming growth factor  $\beta$  (TGF $\beta$ 1) as a key pro-fibrotic growth factor regulates fibroblast proliferation, *trans*-differentiation of fibroblast to myofibroblast, and collagen deposition during fibrosis through the canonical signaling pathway with activation of smad2/3, and non-canonical signaling pathway, such as wnt/ $\beta$ -catenin pathway.<sup>6,7</sup>

Cyclic nucleotide phosphodiesterase (PDEs) are cellular enzymes that catalyze the hydrolysis of 2-s messengers, cyclic adenosine monophosphate (cAMP) and cyclic guanosine monophosphate (cGMP), which play important roles in regulating numerous cellular functions in physiology and pathology of the lung.<sup>8,9</sup> Public dataset analysis also suggested that cAMP signaling pathway and cGMP-PKG signaling pathway involved in bleomycin induced lung fibrosis.<sup>10</sup> Previous studies have shown that PDE4 inhibitor and PDE5 inhibitor play the inhibitory roles on lung fibrosis and ECM formation.<sup>11,12</sup> PDE4 is the cAMP-specific PDEs, PDE5 is cGMP-specific PDEs, whereas PDE10A is both cAMP and cGMP-specific PDEs (14, 15). Recently, it demonstrated that pan-PDE inhibitors represent promising anti-fibrotic effects in human lung fibroblasts.<sup>13</sup> However, the role of PDE10A in PF has not been evaluated.

Papaverine (6,7-dimethoxy-1-veratryl-isoquinoline) is a non-narcotic opium alkaloid isolated from *papaverine somniferum*, the opium poppy. In clinic, papaverine as a PDE10A inhibitor is often used as a

<sup>1</sup>Department of Pharmacology and Sir Run Run Shaw Hospital, Zhejiang University School of Medicine, Hangzhou, Zhejiang 310058, China

<sup>2</sup>Department of Clinical Laboratory, Children's Hospital, Zhejiang University School of Medicine, National Clinical Research Center for Child Health, Hangzhou, Zhejiang 310003, China

<sup>3</sup>Department of Thoracic Surgery, First Affiliated Hospital, Zhejiang University School of Medicine, Hangzhou, Zhejiang 310003, China

<sup>4</sup>Department of Anesthesiology, Women's Hospital, Zhejiang University School of Medicine, Hangzhou, Zhejiang 310006, China

<sup>5</sup>Clinical Laboratory, Sir Run Run Shaw Hospital, Zhejiang University School of Medicine, and Key Laboratory of Precision Medicine in Diagnosis and Monitoring Research of Zhejiang Province, Hangzhou, Zhejiang 310016, China

<sup>6</sup>These authors contributed equally

<sup>7</sup>Lead contact

\*Correspondence:

tanghuifang@zju.edu.cn

<https://doi.org/10.1016/j.isci.2023.106586>



vasodilator and smooth muscle relaxant in condition associated with spasm by regulating cAMP and cGMP.<sup>14–16</sup> In recent years, growing reports on papaverine have focused on anti-tumor and neuronal cells protection. The main mechanism involved is that inhibition of PDE10A promotes the activation of cGMP-PKG pathway, and further inhibits the wnt/ $\beta$ -catenin pathway, thereby inhibiting the proliferation and promoting apoptosis of pulmonary vascular endothelial cells and colorectal cancer cells.<sup>17,18</sup> In psychiatric disorders, the protective effects on neurons include inhibition of PDE10A followed by further inhibition of oxidative stress via cAMP/PKA signaling pathway.<sup>19,20</sup> Of interest, vasodilator-stimulated phosphoprotein (VASP) is an actin regulatory protein that functions in adhesion and migration, commonly as a classical downstream marker of PKA and PKG activity,<sup>21</sup> whereas VASP is also a non-canonical downstream molecule of wnt/ $\beta$ -catenin pathway.<sup>22</sup> However, the potential of papaverine in PF has not been elaborated.

In this study, we first identified the specific expression of PDE10A in fibroblasts/myofibroblasts and PF tissues, and investigated the potential effect and mechanism of PDE10A in PF. *In vitro* experiments, we found that papaverine inhibited myofibroblasts differentiation, and *in vivo* experiments, confirmed effect of papaverine on bleomycin (BLM)-induced PF and amiodarone-induced oxidative stress. In addition, papaverine specifically inhibits the  $\beta$ -catenin/VASP pathway alleviating the fibrosis process.

## RESULTS

### PDE10A gene expression in lung fibrosis from public data source

To definite PDE10A expression in lung tissue of IPF patients and bleomycin induced mouse lung fibrosis model, we reanalyzed the published single-cell RNA-seq data, which from patients with PF (GSE122960)<sup>23</sup> and mice exposed to bleomycin (GSE104154),<sup>24</sup> and found that PDE10A specifically express in fibroblast and myofibroblast, except smooth muscle or endothelial cells (Figures 1A–1D). Those results are consistent with previous literatures, PDE10A expression upregulated in smooth muscle and endothelia cell, which contributes to pulmonary vascular remodeling, and papaverine have protective effect in monocrotaline induced pulmonary hypertensive rats.<sup>25</sup> Meanwhile, the expression level of PDE10A in myofibroblast was significantly higher than that in fibroblast. So, those results suggested that PDE10A may be a good target for PF.

### PDE10A contributes to myofibroblast activation and pulmonary fibrosis

To validate PDE10A expression in human fibroblast and lung tissue of bleomycin model, then we selected TGF $\beta$ 1-induced fibroblast differentiation as cell model to determine the effect of PDE10A expression on myofibroblast activation, and prepared the bleomycin induced lung fibrosis model to determine the lung tissue. HFL-1 cells were treated with TGF $\beta$ 1 (10 ng/mL) for 48 h, 72 h and 96 h. The results showed that TGF $\beta$ 1 significantly upregulated the mRNA expression of myofibroblast markers at 48 h, such as Col I (Figure 1F) and  $\alpha$ -SMA (Figure 1G), by 6.8- and 9.3-fold, respectively. Meanwhile, the mRNA of PDE10A also peaked at 48 h (2.4-fold) (Figure 1H). Those results suggested that PDE10A promote myofibroblast activation. To confirm the effect of PDE10A in myofibroblast activation, we used exogenous PDE10A over-expressed plasmids in HFL-1 cells and determined by His tag. The results showed that PDE10A overexpression could upregulate the expression of myofibroblast markers, such as FN, Col I and  $\alpha$ -SMA by 1.3, 2.8 and 3.7-folds, respectively, and could mimic TGF $\beta$ 1 treatment (Figure 1I).

To further confirm the expression of PDE10A in lung from bleomycin (BLM, 4 U/kg)-induced PF model, at different timepoints day 7, 14, 21, we collected the lung and determined the PDE10A mRNA expression. The highest expression was found during the fibrotic process (14 and 21 days) but not during the inflammatory process (7 days) (Figures 1K and 1L). Those results suggested that PDE10A participates in the myofibroblast activation and development of PF.

### PDE10A inhibitor papaverine inhibits TGF $\beta$ 1-induced fibroblasts activation

To confirm the potential role of PDE10A in PF, we examined the inhibitory effect of papaverine, an old drug with PDE10 inhibition, on TGF $\beta$ 1-induced myofibroblast differentiation cell model. WB results also confirmed that papaverine (100  $\mu$ M) markedly repressed TGF $\beta$ 1-induced  $\alpha$ -SMA, Col I and FN expression by 66%, 81% and 65%, respectively, parallel to the decrease of PDE10A (Figure 2B). qPCR results showed that papaverine decreased TGF $\beta$ 1 elevated mRNA level of  $\alpha$ -SMA, FN, Col I and Col III in a dose-dependent manner (Figures 2C–2F). In addition, myofibroblast differentiation was observed by immunofluorescence assay for  $\alpha$ -SMA expression, and the results is consistent with WB in fibroblasts HFL-1 (Figure 2G). To further confirm the effect of PDE10A, we additionally selected a selective small molecule inhibitor of



**Table 1. Primer sequences used in this study**

The primer	Primer sequences
h $\alpha$ -SMA	Forward: GTG TTG CCC CTG AAG AGC AT Reverse: GCT GGG ACA TTG AAA GTC TCA
h PDE10A	Forward: GAG ACA ACC AGC TACTCC TCT Reverse: ACA GGC TAT TAT TGC ACT CTC CA
h FN	Forward: AAA CCT CGG CTT CCT CCA TAA Reverse: AGG ACG CTC ATA AGT GTC ACC
h Col1a1	Forward: GTG CGA TGA CGT GAT CTG TGA Reverse: CGG TGG TTT CTT GGT CGG T
h Col3a1	Forward: GCC AAA TAT GTG TCT GTG ACT CA Reverse: GGG CGA GTA GGA GCA GTT G
h $\beta$ -catenin	Forward: CAT CTA CAC AGT TTG ATG CTG CT Reverse: GCA GTT TTG TCA GTT CAG GGA
h VASP	Forward: CGG GCT ACT GTG ATG CTT TAT G Reverse: TAG CAG TGG GGT TGT GGT AGA
h LEF1	Forward: TGT TTA TCC CAT CAC GGG TGG Reverse: CAT GGA AGT GTC GCC TGA CAG
h DKK1	Forward: CTC ATC AAT TCC AAC GCG ATC A Reverse: GCC CTC ATA GAG AAC TCC CG
h GAPDH	Forward: GGA GCG AGA TCC CTC CAA AAT Reverse: GGC TGT TGT CAT ACT TCT CAT GG
m FN	Forward: ATG TGG ACC CCT CCT GAT AGT Reverse: GCC CAG TGA TTT CAG CAA AGG
m Col1a2	Forward: CCA GCG AAG AAC TCA TAC AGC Reverse: AAT GTC CAG AGG TGC AAT GTC
m $\alpha$ -SMA	Forward: GTC CCA GAC ATC AGG GAG TAA Reverse: TCG GAT ACT TCA GCG TCA GGA
m $\beta$ -actin	Forward: GAT TAC TGC TCT GGC TCC TAG C Reverse: GAC TCA TCG TAC TCC TGC TTG C

### Papaverine retards the progression of pulmonary fibrosis in mice model

Based on the expression of PDE10A in the lung of bleomycin model, we administrated papaverine (4 mg/kg) or pirfenidone (100 mg/kg) from D7 up to D21 in bleomycin mice model (Figure 3A). Compared to controls, the body weight significantly decreased from D0 to D7 in bleomycin-induced mice, whereas mice receiving papaverine treatment rapidly entered the recovery phase, whereas mice receiving pirfenidone did not show the significant recovery (Figure 3B). By day 21, bleomycin induced significant fibrotic pathological manifestations, including thickening of the alveolar walls and deposition of severe fibroblast foci, whereas papaverine could significantly improve lung structure and reduced collagen deposition, slightly better than the effect of pirfenidone (Figures 3C and 3D). Ashcroft fibrosis scores also supported this observation (Figure 3E). Meanwhile, papaverine or pirfenidone significantly reduced the soluble collagen in lung tissue (Figure 3F). Papaverine also significantly reduced protein expression of FN and  $\alpha$ -SMA by 93% and 72%, respectively (Figure 3G). In addition, papaverine down-regulated mRNA expression of fibrotic genes, such as FN, Col I and  $\alpha$ -SMA, whereas pirfenidone as a positive drug also significantly downregulated the mRNA levels of myofibroblast activation markers on FN, but not Col I and  $\alpha$ -SMA (Figures 3H–3J). So, papaverine may be better than pirfenidone on the recovery of bodyweight and development of fibrosis.

In addition, considering the anti-oxidant effect of pirfenidone in PF,<sup>26</sup> we also prepared amiodarone-induced PF model which was characterized by increased ROS and thickened alveolar wall which may originate from hypertrophic epithelial cells.<sup>27,28</sup> Papaverine and pirfenidone did not change the bodyweight tendency

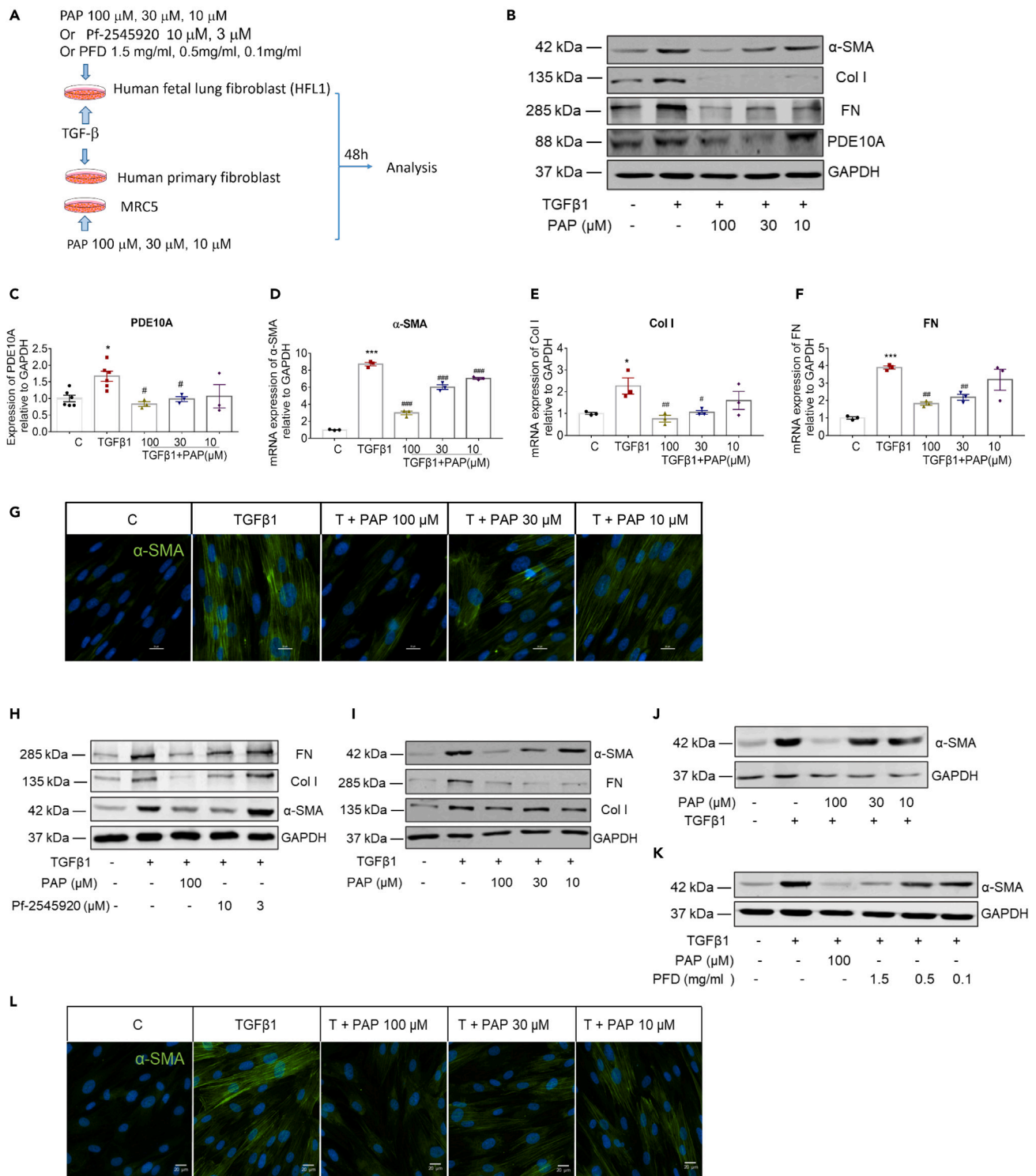


**Figure 2. Papaverine inhibits TGF $\beta$ 1-induced fibroblasts activation**

(A) The diagram for cell experiment.

(B–G) HFL-1 cells were treated at concentrations of 100  $\mu$ M, 30  $\mu$ M or 10  $\mu$ M of papaverine combined with treatment of TGF $\beta$ 1 for 48 h. The expression of PDE10A and myofibroblast marker, including  $\alpha$ -SMA, Col I and FN, was also measured by western blotting (B). mRNA expression of myofibroblast markers, including PDE10A (C)  $\alpha$ -SMA (D), Col I (E) and FN (F), was performed by qPCR in HFL-1. Primer sequence see Table 1. Densitometry data are shown as

**Figure 2. Continued**

means  $\pm$  SEM, n = 3, \*p < 0.05 versus control. #p < 0.05 versus TGF $\beta$ 1. Representative image of TGF $\beta$ 1-induced  $\alpha$ -SMA and inhibition by papaverine in HFL-1 by immunofluorescence assay(G).

(H) PDE10A specific inhibitor Pf-2545920 inhibits myofibroblast differentiation and downregulates expression of  $\beta$ -catenin/VASP. HFL-1 cells were pre-treated with papaverine (100  $\mu$ M) or Pf2545920 (10  $\mu$ M or 3  $\mu$ M) followed by stimulation with TGF $\beta$ 1 induction for 48 h and detected FN, Col I and  $\alpha$ -SMA by WB assay.

(I) Human-derived lung fibroblasts (LFs) were pre-incubated with 100  $\mu$ M, 30  $\mu$ M or 10  $\mu$ M of papaverine subsequently stimulated with TGF $\beta$ 1 (10 ng/mL) for 48 h.  $\alpha$ -SMA, FN and Col I protein expression was measured in LFs by WB assay.

(J) Papaverine inhibits TGF $\beta$ 1-induced fibroblast-to-myofibroblast transition in MRC-5. MRC-5 cells were starved for 24 h and then treatment with TGF $\beta$ 1 (10 ng/mL) or TGF $\beta$ 1+papaverine (100  $\mu$ M, 30  $\mu$ M or 10  $\mu$ M) for 48 h.  $\alpha$ -SMA protein expression was measured in MRC-5 by WB assay.

(K) Pirfenidone inhibits TGF $\beta$ 1-induced myofibroblast differentiation in HFL-1. HFL-1 cells was starved for 24 h and then treatment with TGF $\beta$ 1 (10 ng/mL) or TGF $\beta$ 1+papaverine (100  $\mu$ M) and TGF $\beta$ 1+pirfenidone (1.5 mg/mL, 0.5 mg/mL or 0.1 mg/mL) for 48 h.  $\alpha$ -SMA protein expression was measured in HFL-1 by WB assay.

(L) Representative image and quantification of TGF $\beta$ 1-induced  $\alpha$ -SMA and inhibition by papaverine in MRC-5 by immunofluorescent assay.

(Figure 4B), but can reverse the decreased SOD activity and increased MDA levels (Figures 4C and 4D), meanwhile, they significantly decreased the alveolar wall thickness (Figures 4E and 4G). There were little changes of soluble collagen in lung tissue after papaverine and pirfenidone treatment (Figure 4F), it may be because of the lack of obvious intra-alveolar fibrosis in AD model.<sup>28</sup> Previous report also suggested that pirfenidone was also lack of effectiveness on collagen, after using from 7nd day in amiodarone model.<sup>29</sup> Those results suggested that papaverine also have anti-oxidant effects. Based on the similar effect of papaverine and pirfenidone, papaverine may be a candidate for the lung fibrosis therapy.

**Papaverine inhibits TGF $\beta$ 1 upregulated VASP expression**

Previous studies have proved that papaverine plays a pharmacological role in central nervous diseases and erectile dysfunction diseases by targeting PDE10A to upregulate second messenger cAMP and/or cGMP.<sup>30,31</sup> To test the action of papaverine on PDE10A, we measured intracellular cAMP and cGMP levels, and the results showed that papaverine significantly elevated cAMP and cGMP, and the baseline content of cAMP was higher in lung fibroblasts (Figures 5B and 5C), which may be related to the higher concentration of cAMP.<sup>32</sup> The main downstream effector of cAMP and cGMP are PKA and PKG, two phosphorylation sites of VASP, serine 157 residues (p-VASP-157) and serine 239 residue (p-VASP-239) are often used to evaluate the activation of PKA and PKG, respectively.<sup>21,33</sup> Of interest, p-VASP-157, p-VASP-239 and total VASP expression showed a marked increase after TGF- $\beta$ 1 stimulation, whereas papaverine decreased the total VASP expression in concentration-dependent manner (Figures 5D and 5E). In previous reports, PDE10A inhibitor increased the phosphorylated VASP in colon tumor cells, such as HT-29, SW-480, and HCT-116.<sup>18</sup> However, our results suggested that VASP decrease on myofibroblast transformation by papaverine is different with the previous reports. Therefore, we confirmed the effect of papaverine on total VASP on the SW480 cell. The results showed that VASP expression was unchanged (Figure 5F). So, those results suggested that the regulation of VASP in fibroblast is different with cancer cells.

To confirm the action of VASP in fibroblasts activation, we further knockdown VASP with specific siRNA, the results showed that si-VASP inhibited TGF $\beta$ 1 induced myofibroblast activation, decreased Col I and  $\alpha$ -SMA (Figure 5G). Moreover, in the lung tissue of the bleomycin model, VASP increased 2.1-fold than control, papaverine and pirfenidone significantly reduced VASP expression by 48% and 58%, respectively (Figure 5H), accompanied by a decrease of FN and  $\alpha$ -SMA (Figure 3G). All those data indicated VASP can be the unique target on the myofibroblast activation.

**Papaverine inhibits TGF $\beta$ 1 upregulated  $\beta$ -catenin/VASP signaling**

Of interest, except as a classic downstream marker of PKA and PKG activity,<sup>21</sup> VASP is also a non-canonical downstream molecule of wnt/ $\beta$ -catenin pathway.<sup>22</sup> So, we raise the hypothesis that papaverine inhibit the lung fibrosis by  $\beta$ -catenin/VASP pathway. To confirm our hypothesis, we first overexpressed PDE10A plasmid, and then to determine the protein expression of  $\beta$ -catenin and VASP. The results showed that PDE10A overexpression up-regulated  $\beta$ -catenin and VASP, which was similar with the action of TGF $\beta$ 1 (Figure 6B), suggesting that  $\beta$ -catenin/VASP mediated PDE10A induced fibroblasts activation. We further determined the effect of papaverine on  $\beta$ -catenin/VASP pathway, and found that papaverine significantly inhibited TGF $\beta$ 1-induced upregulation of  $\beta$ -catenin and VASP in dose-dependent manners.

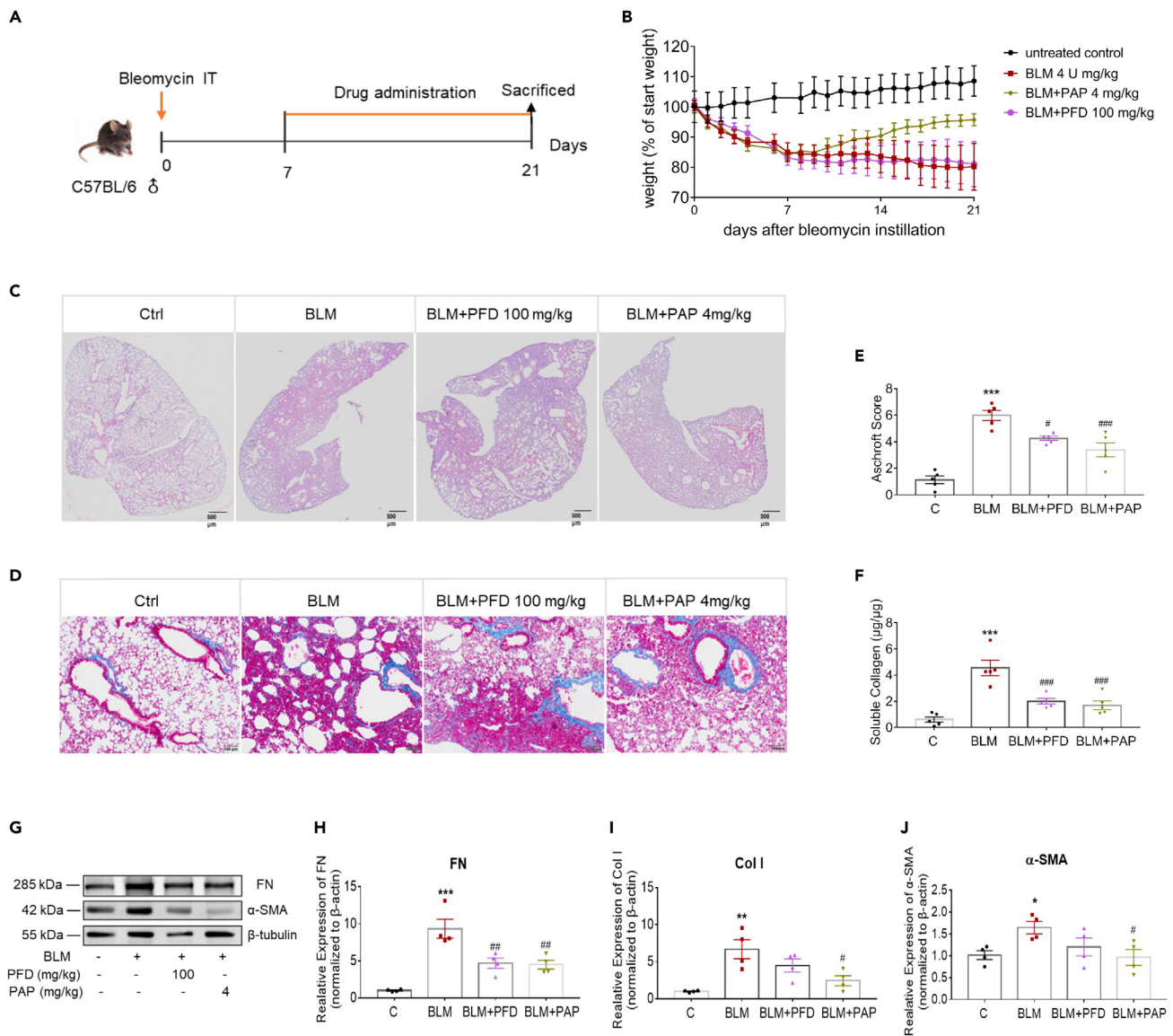


**Figure 3. Papaverine attenuates bleomycin-induced lung fibrosis in mice**

(A) Diagram of animal modeling. C57BL/6 mice received intratracheal instillation of sodium chloride (C, n = 5) or 4 U/kg bleomycin (BLM, n = 15). Treatment was performed by daily intraperitoneal injection of papaverine (4 mg/kg) as well as pirfenidone (100 mg/kg) (n = 5) from day 7 to day 21.

(B) Body weight is expressed as % of starting weight.

(C) Representative panorama images from mouse lungs of HE staining. scale bar = 500 µm.

(D) Representative images from mouse lungs of Masson trichrome staining. scale bar = 100µm.

(E) Ashcroft score.

(F) Soluble collagen in lung tissue was measured by Sircol Soluble Collagen Assay.

(G) Protein expression of FN and α-SMA were performed by WB.

(H–J) mRNA expression of myofibroblast differentiation markers FN (H), Col I (I) and α-SMA (J) in lung tissues were performed by qPCR. Primer sequence see Table 1. Data shown are means ± SEM of n = 4–5. \*\*p < 0.01 versus control. #p < 0.05, ##p < 0.01 versus BLM group. BLM: bleomycin; PAP: papaverine; PFD: pirfenidone.

In addition, analysis of β-catenin distribution in the cytoplasm and nucleus also showed significant inhibition, the inhibitory percent was 68 and 58% at 100 µM, respectively (Figure 6C). We further determined the effect of PDE10A selective inhibitor Pf-2545920, and got the similar inhibitory effect (Figure 6D). Those results suggested that PDE10A inhibition can decrease the TGFβ1-induced the upregulation of β-catenin/VASP.

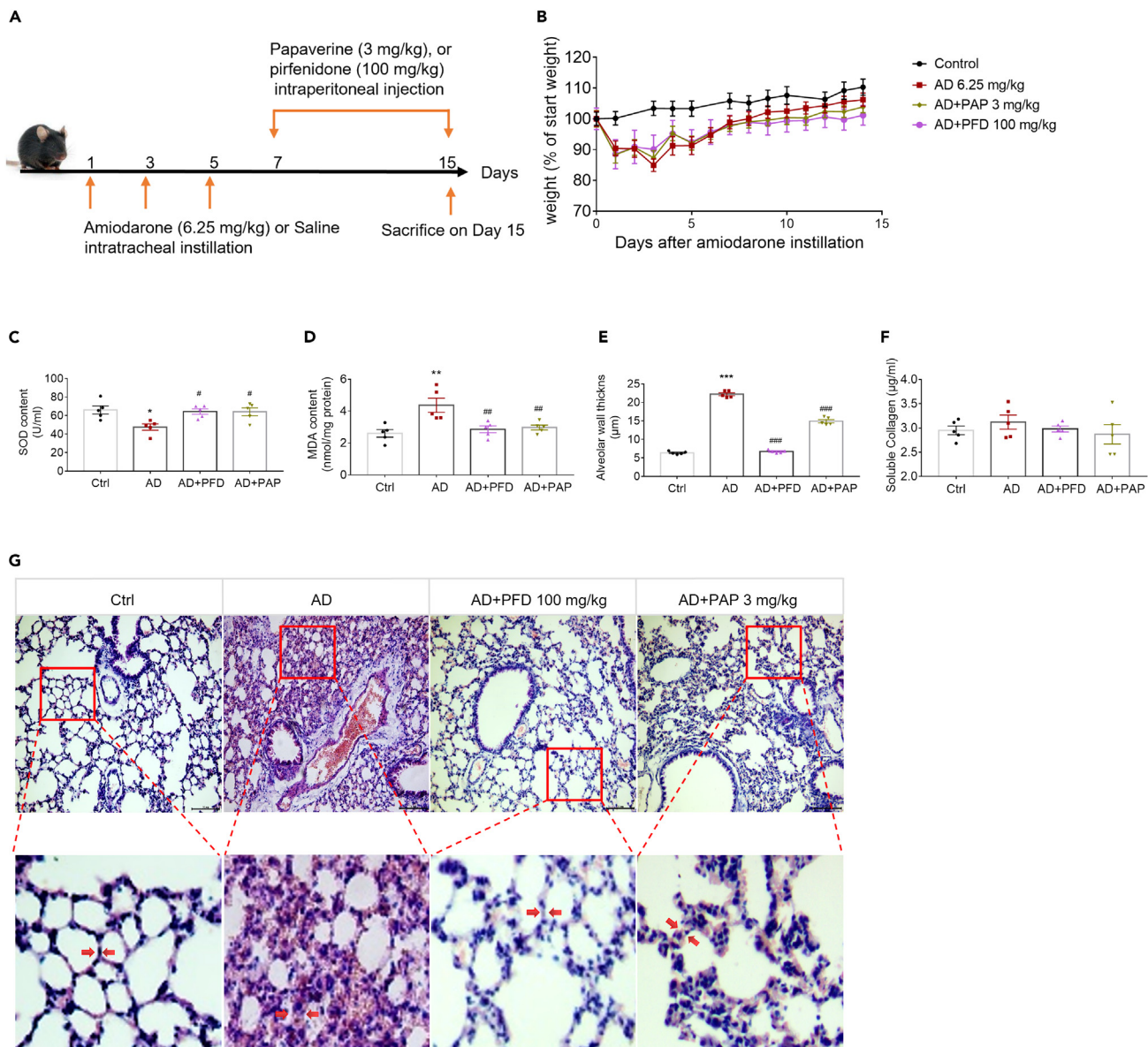


**Figure 4. Papaverine attenuates amidarone-induced oxidative stress in mice**

(A) Diagram of animal modeling. C57BL/6 mice received intratracheal instillation of sodium chloride (C, n = 5) or 6.25 mg/kg amidarone (AD, n = 15). Treatment was performed by daily intraperitoneal injection of papaverine (3 mg/kg) as well as pirfenidone (100 mg/kg) (n = 5) from day 7 to day 15. (B) Body weight is expressed as % of starting weight. (C) SOD in lung tissue was measured by SOD kits. (D) MDA in lung tissue was measured by MDA kits. (E) Alveolar wall thickness was determined by ImageJ. (F) Soluble collagen in lung tissue was measured by Sircol Soluble Collagen Assay. (G) Representative images from mouse lungs of Masson trichrome staining. scale bar = 100  $\mu$ m. Densitometry data are shown as means  $\pm$  SEM, n = 5, \*\*\*p < 0.001 versus control. ###p < 0.001 versus AD group. AD: amidarone; PAP: papaverine; PFD: pirfenidone.

To confirm the direct effect of  $\beta$ -catenin inhibition, we treated HFL-1 with ICG-001, an inhibitor of the wnt/ $\beta$ -catenin pathway, and found that ICG-001 also significantly suppressed the phenotypic molecules expression of myofibroblast activation, such as Col I,  $\alpha$ -SMA, FN, as well as VASP (Figure 6E). Meanwhile, papaverine significantly downregulated the mRNA levels of the downstream molecules of  $\beta$ -catenin, such as DKK-1 (Dickkopf WNT Signaling Pathway Inhibitor 1) and LEF1 (Lymphoid Enhancer Binding Factor 1) in dose dependent manners (Figure 6F). Silencing VASP by siRNA also decreased the mRNA expression of FN, COL I,  $\beta$ -catenin,

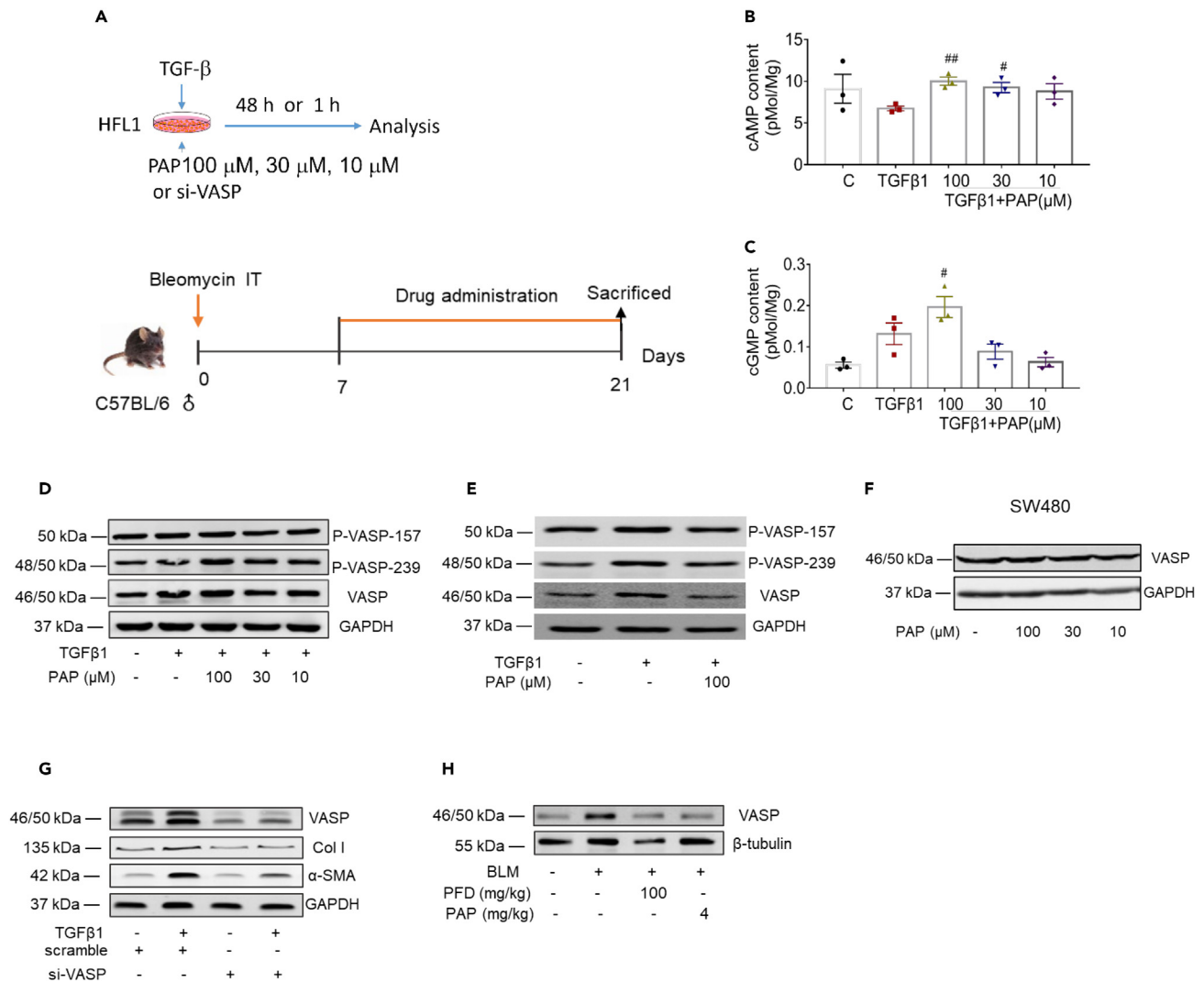


**Figure 5. Papaverine inhibits VASP expression**

(A) Diagram of this part. For cell part, HFL-1 cells were starved for 24 h and then treatment with TGFβ1 (10 ng/mL) or TGFβ1+papaverine (100 μM, 30 μM, 10 μM) for 48 h.

(B and C) cAMP and cGMP level in HFL-1 cells were determined by cAMP and cGMP kit. Densitometry data are shown as means ± SEM, n = 3, #p < 0.05 versus TGFβ1 group. \*p < 0.05 versus control.

(D) Phosphorylation of p-157 and p-239 sites of VASP, papaverine was measured by WB assay at 1 h.

(E) Activation of the p-157 and p-239 phosphorylation sites of VASP by papaverine was measured by WB assay at 48 h.

(F) The effect of papaverine on VASP expression was examined in SW480 cells.

(G) HFL-1 cells were transfected by VASP siRNA or scramble siRNA for 6 h and then cultured with TGFβ1 treatment for another 48 h. VASP, Col I and α-SMA protein expression was measured by WB.

(H) The expression of VASP in the lung of bleomycin induced model was detected by WB.

LEF-1 and DKK-1, suggested that VASP may be required for fibrotic remodeling of lung (Figure 6G). To confirm the direct interaction between VASP and β-catenin, we used co-IP to pull down VASP, then to determine β-catenin. The results suggested that β-catenin and VASP can form a complex (Figures 6H and 6I). Therefore, those results suggested that papaverine inhibit fibroblasts activation by down-regulating β-catenin/VASP pathway.

## DISCUSSION

In this study, we demonstrated for the first time that PDE10A specific up-regulated in PF, and promote myofibroblast activation. In addition, PDE10A inhibitor papaverine prevented PF, including inhibiting TGFβ1 induced fibroblast differentiation, anti-fibrotic and anti-oxidant effects, providing evidence for the therapeutic

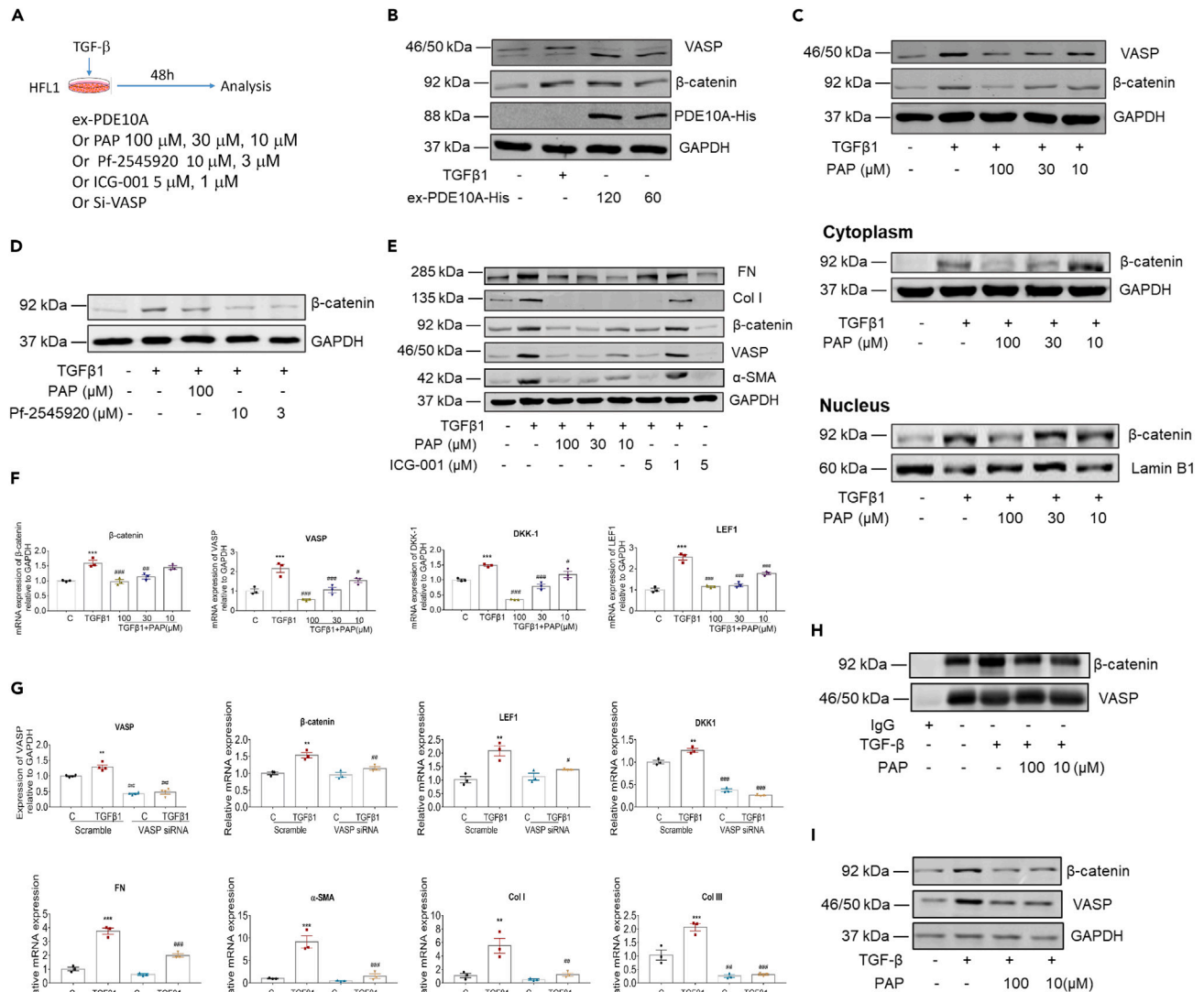


**Figure 6. Papaverine inhibits TGF $\beta$ 1-induced myofibroblast differentiation in HFL-1 mediated by  $\beta$ -catenin/VASP pathway**

(A) Diagram of this part. For cell part, HFL-1 cells were starved for 24 h and then treatment with TGF $\beta$ 1 (10 ng/mL) or other treatment for 48 h.

(B) After transfection of adenoviral vector encoding PDE10A (MOI= 120 or 80) for 12 h, HFL-1 cells were starved for 24 h. The control cells were stimulated with TGF $\beta$ 1 (10 ng/mL) for 48 h and then detected the expression of PDE10A,  $\beta$ -catenin and VASP by WB.

(C) HFL-1 cells were treated at concentrations of 100  $\mu$ M, 30  $\mu$ M or 10  $\mu$ M of papaverine combined with treatment of TGF $\beta$ 1 for 48 h, and then  $\beta$ -catenin and VASP were determined by WB. The nuclear translocation of  $\beta$ -catenin was detected by separating the nucleus from the cytoplasm of the protein.

(D) PDE10A specific inhibitor Pf-2545920 inhibits myofibroblast differentiation and downregulates expression of  $\beta$ -catenin/VASP. HFL-1 cells were pre-treated with papaverine (100  $\mu$ M) or Pf2545920 (10  $\mu$ M or 3  $\mu$ M) followed by stimulation with TGF $\beta$ 1 induction for 48 h and detected by WB assay.

(E) HFL-1 cells were starved for 24 h and then detected the  $\beta$ -catenin after treatment with wnt/ $\beta$ -catenin pathway inhibitor ICG-001 (5  $\mu$ M or 1  $\mu$ M) or papaverine (100  $\mu$ M, 30  $\mu$ M or 10  $\mu$ M) by WB.

(F) The mRNA levels of VASP,  $\beta$ -catenin, DKK-1, LEF1 were detected by qPCR. Data are shown as means  $\pm$  SEM, n = 3, \*p < 0.05 versus scramble control. #p < 0.05 versus scramble TGF $\beta$ 1.

(G) HFL-1 cells were transfected by VASP siRNA or scramble siRNA for 6 h and then cultured with TGF $\beta$ 1 treatment for another 48 h. The mRNA levels of VASP and  $\beta$ -catenin pathway related molecules (VASP,  $\beta$ -catenin, DKK-1, LEF1) were detected by qPCR. Primer sequence see Table 1. Data are shown as means  $\pm$  SEM, n = 3, \*p < 0.05 versus scramble control. #p < 0.05 versus scramble TGF $\beta$ 1.

(H and I) HFL-1 cells were treated at concentrations of 100  $\mu$ M, 10  $\mu$ M of papaverine combined with treatment of TGF $\beta$ 1 for 48 h, co-IP results.

effect of PDE10A inhibitor on PF. The mechanism of action of PDE10A inhibitor mediated by the  $\beta$ -catenin/VASP pathway. Our study confirmed the effect of papaverine in PF, opening a new avenue for this old drug. In addition, we found the fibrogenic function of VASP which could be the unique target on myofibroblast activation.

The pathogenesis of PF is complex, involving not only fibroblasts cell proliferation and transformation, but also a series of pathologies, including oxidative stress profiles.<sup>34,35</sup> The specific expression of PDE10A in fibroblasts and myofibroblasts suggested it will be a good target for PF. In our *in vitro* experiments, we confirmed the effectiveness of PDE10A inhibitor papaverine and Pf-2545920 on myofibroblast activation. In our *in vivo* experiments, we confirmed the effects of papaverine in bleomycin-induced fibrosis, and found that papaverine and pirfenidone exhibited similar inhibitory trends on bleomycin-induced PF and ECM formation. Meantime, papaverine may be better than pirfenidone on the recovery of bodyweight and development of fibrosis in bleomycin induced model. Another PF model, amiodarone induced PF model, characterized by decreased SOD activity and increased MDA, papaverine and pirfenidone also exhibited similar inhibitory trends, decreased the oxidation levels, and retarded the pathological changes, but in here, pirfenidone may be better than papaverine on alveolar wall thickness which because of the epithelial hypertrophy. From the distribution of PDE10A in lung, we found that PDE10A specifically express in fibroblast and myofibroblast, except smooth muscle or endothelial cells, that means PDE10A inhibitor may lack the activity on epithelial cell, whereas pirfenidone have more potency on epithelial cell.<sup>36</sup> However, the distribution of PDE10A in endothelial cells and smooth muscle may also bring beneficial effects on the treatment of PF. Previous reports suggested that papaverine could inhibit overproduction of extracellular connective tissue elements in smooth muscle cells, then prevented mechanical stimulation induced venous injury,<sup>37</sup> meanwhile, papaverine could attenuate hemodynamic parameter and pulmonary vascular remodeling in monocrotaline induced pulmonary hypertensive in rats.<sup>25</sup> That may suggest the PDE10A inhibition maybe exert the anti-fibrotic and anti-oxidant effect on the process of lung fibrosis.

Previous studies supported PDE10A may contribute to impairments in the central nervous system (CNS) function, including cognitive deficits, disturbances of behavior, emotion processing, and movement. Potential utility of PDE10A inhibitors for the treatment of CNS-related disorders, such as schizophrenia as well as Huntington's and Parkinson's diseases, has been more widely reported.<sup>30</sup> Papaverine as the first marketed PDE10A inhibitor since 1933 has been approved for clinical use in visceral spasm, vasospasm and erectile dysfunction. And the side effect includes ventricular tachycardia, diarrhea, somnolence, vertigo, flushing and headache. But the selectivity of papaverine on PDE10A is not very high, the IC<sub>50</sub> for PDE10A is 36 nM,<sup>38</sup> whereas Pf-2545920 is a high selectivity, IC<sub>50</sub> for PDE10A is 0.37 nM,<sup>39</sup> 100-folds of papaverine. But in our results, the effect of 10  $\mu$ M Pf-2545920 was similar with 100  $\mu$ M papaverine (Figures 2H and 6D), that also suggested that papaverine have other action beyond PDE10A inhibition. Moreover, the molecular imaging of PDE10A by PET had been used to determine the function of brain.<sup>40</sup> If possible, PDE10A can be also used to determine the changes of PF, or pulmonary hypertension.

Human VASP is a weakly processive actin polymerase, involved in the inhibition of agonist-induced platelet aggregation by cyclic nucleotides, and the adhesion of platelets to the vascular wall.<sup>33</sup> Although the literature has shown that VASP level in the peribiliary vascular plexus of cirrhotic rats is significantly upregulated,<sup>41</sup> no reports have directly demonstrated the role of VASP in PF. In this study, we found that PDE10A overexpression significantly increased the protein level of VASP, whereas VASP knockdown not only reduced the downstream molecules of wnt/ $\beta$ -catenin pathway, but also inhibited the expression of myofibroblast differentiation-related proteins and cell proliferation. It suggested that that  $\beta$ -catenin/VASP plays an important role for papaverine on inhibition of myofibroblast activation and proliferation. In tumor-related studies, PDE10A inhibition increased cGMP/PKG then decreased the wnt/ $\beta$ -catenin pathway through significantly activating phosphorylation of  $\beta$ -catenin at Ser552 site, whereas increasing the cAMP/PKA to phosphorylate Ser675 site of  $\beta$ -catenin did not inhibit cell proliferation.<sup>42,43</sup> However, in PF, extensive literature supported that activated wnt/ $\beta$ -catenin pathways not only play an important role in the excessive proliferation of epithelial cells and fibroblasts, but also trigger myofibroblast differentiation.<sup>44,45</sup> In addition, the wnt/ $\beta$ -catenin pathway inhibits cancer cell proliferation by interacting with VASP.<sup>46,47</sup> Recently published studies showed that wnt/ $\beta$ -catenin/VASP forms a malignant positive feedback loop in breast cancer and promotes the proliferation and migration of breast cancer cells.<sup>48</sup> So  $\beta$ -catenin/VASP pathway should be a critical way to regulate differentiation and proliferation in fibroblast.

In conclusion, our study found that PDE10A could regulate myofibroblasts differentiation and involve in development of PF. PDE10A inhibitor papaverine inhibits myofibroblasts differentiation *in vitro* and alleviates bleomycin-induced PF *in vivo*. And  $\beta$ -catenin/VASP pathway mediated the process. Hence, our data supported that PDE10A maybe a specific therapeutic target of PF and papaverine may be a potential candidate for the treatment of PF.

### Limitations of the study

In this study, we did not confirm the expression and distribution of PDE10A in the lung of clinical IPF patients or donors. Meanwhile, we showed only one dose of papaverine in mice work for the dose-effect relationship is not very significant.

### STAR★METHODS

Detailed methods are provided in the online version of this paper and include the following:

- [KEY RESOURCES TABLE](#)
- [RESOURCE AVAILABILITY](#)
  - Lead contact
  - Materials availability
  - Data and code availability
- [EXPERIMENTAL MODEL AND SUBJECT DETAILS](#)
  - Animals
  - Bleomycin induced lung fibrosis model
  - Amiodarone induced lung fibrosis model
- [METHOD DETAILS](#)
  - PDE10A gene expression validation in public data source
  - Cell culture and treatment
  - Adenovirus cell transfection
  - Immunofluorescence
  - The cAMP and cGMP measurement
  - Histological assessment of lung fibrosis model
  - Soluble collagen assay
  - Oxidative stress indexes
  - RNA isolation and RT-qPCR
  - $\beta$ -catenin nuclear translocation
  - Immunoprecipitation (IP) assay
  - Western blot analysis
- [QUANTIFICATION AND STATISTICAL ANALYSIS](#)

### ACKNOWLEDGMENTS

This study was supported by the National Natural Science Foundation of China grants (No: 81402989, 81570056 and 81170536) and the Natural Science Foundation of Zhejiang Province, China (Grant No. LGD20H010002 and LY18H310002). We heartily appreciated the Professor Alexander V. Misharin (Division of Pulmonary and Critical Care Medicine, Feinberg School of Medicine, Northwestern University), for they provided the UCSC cell browser-based dataset. We heartily appreciated Professor Yuehai Ke for his key constructive comments for this work. We thank for the technical support by the Core Facilities, Zhejiang University School of Medicine.

### AUTHOR CONTRIBUTIONS

L.Y.J. contributed to methodology, software, validation, formal analysis, investigation, data curation, writing, and visualization. S.J.R. contributed to investigation, resources, conceptualization, project administration and supervision. L.S.C. contributed to methodology, formal analysis, investigation, visualization, and writing. W.L.M. contributed to resources. R.D., L.N., and C.X.W. contributed to methodology, investigation. L.Z.G. contributed to conceptualization, project administration and supervision. T.H.F. contributed to conceptualization, resources, writing, supervision, and project administration.

## DECLARATION OF INTERESTS

The authors declare no competing interests.

## INCLUSION AND DIVERSITY

We support inclusive, diverse, and equitable conduct of research.

Received: September 23, 2022

Revised: January 30, 2023

Accepted: April 3, 2023

Published: April 6, 2023

## REFERENCES

- Samarelli, A., Tonelli, R., Marchioni, A., Bruzzi, G., Gozzi, F., Andrisani, D., Castaniere, I., Manicardi, L., Moretti, A., Tabbi, L., et al. (2021). Fibrotic idiopathic interstitial lung disease: the molecular and cellular key players. *Int. J. Mol. Sci.* 22, 8952. <https://doi.org/10.3390/ijms22168952>.
- Gao, J., Kalafatis, D., Carlson, L., Pesonen, I.H.A., Li, C.X., Wheelock, A., Magnusson, J.M., and Sköld, C.M. (2021). Baseline characteristics and survival of patients of idiopathic pulmonary fibrosis: a longitudinal analysis of the Swedish IPF Registry. *Respir. Res.* 22, 40. <https://doi.org/10.1186/s12931-021-01634-x>.
- Raghu, G., Remy-Jardin, M., Myers, J.L., Richeldi, L., Ryerson, C.J., Lederer, D.J., Behr, J., Cottin, V., Danoff, S.K., Morell, F., et al. (2018). Diagnosis of idiopathic pulmonary fibrosis. An official ATS/ERS/JRS/ALAT clinical practice guideline. *Am. J. Respir. Crit. Care Med.* 198, e44–e68. <https://doi.org/10.1164/rccm.201807-1255ST>.
- Wolters, P.J., Collard, H.R., and Jones, K.D. (2014). Pathogenesis of idiopathic pulmonary fibrosis. *Annu. Rev. Pathol.* 9, 157–179. <https://doi.org/10.1146/annurev-pathol-012513-104706>.
- Ding, Q., Luckhardt, T., Hecker, L., Zhou, Y., Liu, G., Antony, V.B., deAndrade, J., and Thannickal, V.J. (2011). New insights into the pathogenesis and treatment of idiopathic pulmonary fibrosis. *Drugs* 71, 981–1001. <https://doi.org/10.2165/11591490-000000000-00000>.
- Sun, Z., Yang, Z., Wang, M., Huang, C., Ren, Y., Zhang, W., Gao, F., Cao, L., Li, L., and Nie, S. (2020). Paraquat induces pulmonary fibrosis through Wnt/ $\beta$ -catenin signaling pathway and myofibroblast differentiation. *Toxicol. Lett.* 333, 170–183. <https://doi.org/10.1016/j.toxlet.2020.08.004>.
- Zent, J., and Guo, L.W. (2018). Signaling mechanisms of myofibroblastic activation: outside-in and inside-out. *Cell. Physiol. Biochem.* 49, 848–868. <https://doi.org/10.1159/000493217>.
- Schmidt, M., Cattani-Cavaliere, I., Nuñez, F.J., and Ostrom, R.S. (2020). Phosphodiesterase isoforms and cAMP compartments in the development of new therapies for obstructive pulmonary diseases. *Curr. Opin. Pharmacol.* 51, 34–42. <https://doi.org/10.1016/j.coph.2020.05.002>.
- Maurice, D.H., Ke, H., Ahmad, F., Wang, Y., Chung, J., and Manganiello, V.C. (2014). Advances in targeting cyclic nucleotide phosphodiesterases. *Nat. Rev. Drug Discov.* 13, 290–314. <https://doi.org/10.1038/nrd4228>.
- Wang, Y., Hu, S., Shen, L., Liu, S., Wan, L., Yang, S., Hou, M., Tian, X., Zhang, H., and Xu, K.F. (2021). Dynamic observation of autophagy and transcriptome profiles in a mouse model of bleomycin-induced pulmonary fibrosis. *Front. Mol. Biosci.* 8, 664913. <https://doi.org/10.3389/fmolb.2021.664913>.
- Togo, S., Liu, X., Wang, X., Sugiura, H., Kamio, K., Kawasaki, S., Kobayashi, T., Ertl, R.F., Ahn, Y., Holz, O., et al. (2009). PDE4 inhibitors roflumilast and rolipram augment PGE2 inhibition of TGF- $\beta$ 1-stimulated fibroblasts. *Am. J. Physiol. Lung Cell Mol. Physiol.* 296, L959–L969. <https://doi.org/10.1152/ajplung.00508.2007>.
- Zenzmaier, C., Kern, J., Heitz, M., Plas, E., Zwerschke, W., Mattesich, M., Sandner, P., and Berger, P. (2015). Activators and stimulators of soluble guanylate cyclase counteract myofibroblast differentiation of prostatic and dermal stromal cells. *Exp. Cell Res.* 338, 162–169. <https://doi.org/10.1016/j.yexcr.2015.08.014>.
- Wójcik-Pszczola, K., Chłoń-Rzepa, G., Jankowska, A., Ślusarczyk, M., Ferdek, P.E., Kusiak, A.A., Świerczek, A., Pocięcha, K., Koczurkiewicz-Adamczyk, P., Wyska, E., et al. (2020). A novel, pan-PDE inhibitor exerts anti-fibrotic effects in human lung fibroblasts via inhibition of TGF- $\beta$  signaling and activation of cAMP/PKA signaling. *Int. J. Mol. Sci.* 21, 4008. <https://doi.org/10.3390/ijms21114008>.
- Masuku, N.P., Unuofin, J.O., and Lebelo, S.L. (2021). Advances in nanoparticle delivery system for erectile dysfunction: an updated review. *Sex. Med.* 9, 100420. <https://doi.org/10.1016/j.esxm.2021.100420>.
- Hocking, K.M., Putumbaka, G., Wise, E.S., Cheung-Flynn, J., Brophy, C.M., and Komalavilas, P. (2016). Papaverine prevents vasospasm by regulation of myosin light chain phosphorylation and actin polymerization in human saphenous vein. *PLoS One* 11, e0154460. <https://doi.org/10.1371/journal.pone.0154460>.
- Chappie, T.A., Humphrey, J.M., Allen, M.P., Estep, K.G., Fox, C.B., Lebel, L.A., Liras, S., Marr, E.S., Menniti, F.S., Pandit, J., et al. (2007). Discovery of a series of 6,7-dimethoxy-4-pyrroliidylquinazoline PDE10A inhibitors. *J. Med. Chem.* 50, 182–185. <https://doi.org/10.1021/jm060653b>.
- Zhu, B., Lindsey, A., Li, N., Lee, K., Ramirez-Alcantara, V., Canzonieri, J.C., Fajardo, A., Madeira da Silva, L., Thomas, M., Piazza, J.T., et al. (2017). Phosphodiesterase 10A is overexpressed in lung tumor cells and inhibitors selectively suppress growth by blocking  $\beta$ -catenin and MAPK signaling. *Oncotarget* 8, 69264–69280. <https://doi.org/10.18632/oncotarget.20566>.
- Lee, K., Lindsey, A.S., Li, N., Gary, B., Andrews, J., Keeton, A.B., and Piazza, G.A. (2016).  $\beta$ -catenin nuclear translocation in colorectal cancer cells is suppressed by PDE10A inhibition, cGMP elevation, and activation of PKG. *Oncotarget* 7, 5353–5365. <https://doi.org/10.18632/oncotarget.6705>.
- Bhat, A., Tan, V., Heng, B., Chow, S., Basappa, S., Essa, M.M., Chidambaram, S.B., and Guillemin, G.J. (2021). Papaverine, a phosphodiesterase 10A inhibitor, ameliorates quinolinic acid-induced synaptotoxicity in human cortical neurons. *Neurotox. Res.* 39, 1238–1250. <https://doi.org/10.1007/s12640-021-00368-4>.
- Lee, Y.Y., Park, J.S., Leem, Y.H., Park, J.E., Kim, D.Y., Choi, Y.H., Park, E.M., Kang, J.L., and Kim, H.S. (2019). The phosphodiesterase 10 inhibitor papaverine exerts anti-inflammatory and neuroprotective effects via the PKA signaling pathway in neuroinflammation and Parkinson's disease mouse models. *J. Neuroinflammation* 16, 246. <https://doi.org/10.1186/s12974-019-1649-3>.
- Li, Z., Ajdic, J., Eigenthaler, M., and Du, X. (2003). A predominant role for cAMP-dependent protein kinase in the cGMP-induced phosphorylation of vasodilator-stimulated phosphoprotein and platelet inhibition in humans. *Blood* 101, 4423–4429. <https://doi.org/10.1182/blood-2002-10-3210>.
- Li, K., Zhang, J., Tian, Y., He, Y., Xu, X., Pan, W., Gao, Y., Chen, F., and Wei, L. (2020). The Wnt/ $\beta$ -catenin/VASP positive feedback

- loop drives cell proliferation and migration in breast cancer. *Oncogene* 39, 2258–2274. <https://doi.org/10.1038/s41388-019-1145-3>.
23. Reyfman, P.A., Walter, J.M., Joshi, N., Anekalla, K.R., McQuattie-Pimentel, A.C., Chiu, S., Fernandez, R., Akbarpour, M., Chen, C.I., Ren, Z., et al. (2019). Single-cell transcriptomic analysis of human lung provides insights into the pathobiology of pulmonary fibrosis. *Am. J. Respir. Crit. Care Med.* 199, 1517–1536. <https://doi.org/10.1164/rccm.201712-24100C>.
  24. Xie, T., Wang, Y., Deng, N., Huang, G., Taghavifar, F., Geng, Y., Liu, N., Kulur, V., Yao, C., Chen, P., et al. (2018). Single-cell deconvolution of fibroblast heterogeneity in mouse pulmonary fibrosis. *Cell Rep.* 22, 3625–3640. <https://doi.org/10.1016/j.celrep.2018.03.010>.
  25. Tian, X., Vroom, C., Ghofrani, H.A., Weissmann, N., Bieniek, E., Grimminger, F., Seeger, W., Schermuly, R.T., and Pullamsetti, S.S. (2011). Phosphodiesterase 10A upregulation contributes to pulmonary vascular remodeling. *PLoS One* 6, e18136. <https://doi.org/10.1371/journal.pone.0018136>.
  26. Puglisi, S., Torrisi, S.E., Vindigni, V., Giuliano, R., Palmucci, S., Mulè, M., and Vancheri, C. (2016). New perspectives on management of idiopathic pulmonary fibrosis. *Ther. Adv. Chronic Dis.* 7, 108–120. <https://doi.org/10.1177/2040622315624276>.
  27. Taylor, M.D., Van Dyke, K., Bowman, L.L., Miles, P.R., Hubbs, A.F., Mason, R.J., Shannon, K., and Reasor, M.J. (2000). A characterization of amiodarone-induced pulmonary toxicity in F344 rats and identification of surfactant protein-D as a potential biomarker for the development of the toxicity. *Toxicol. Appl. Pharmacol.* 167, 182–190. <https://doi.org/10.1006/taap.2000.9000>.
  28. Li, S., Shi, J., and Tang, H. (2022). Animal models of drug-induced pulmonary fibrosis: an overview of molecular mechanisms and characteristics. *Cell Biol. Toxicol.* 38, 699–723. <https://doi.org/10.1007/s10565-021-09676-z>.
  29. Card, J.W., Racz, W.J., Brien, J.F., Margolin, S.B., and Massey, T.E. (2003). Differential effects of pirfenidone on acute pulmonary injury and ensuing fibrosis in the hamster model of amiodarone-induced pulmonary toxicity. *Toxicol. Sci.* 75, 169–180. <https://doi.org/10.1093/toxsci/kfg167>.
  30. Jankowska, A., Świerczek, A., Wyska, E., Gawalska, A., Bucki, A., Pawłowski, M., and Chłoń-Rzepa, G. (2019). Advances in discovery of PDE10A inhibitors for CNS-related disorders. Part 1 overview of the chemical and biological research. *Curr. Drug Targets* 20, 122–143. <https://doi.org/10.2174/1389450119666180808105056>.
  31. Maggi, M., Filippi, S., Ledda, F., Magini, A., and Forti, G. (2000). Erectile dysfunction: from biochemical pharmacology to advances in medical therapy. *Eur. J. Endocrinol.* 143, 143–154. <https://doi.org/10.1530/eje.0.1430143>.
  32. Weber, M., Breier, M., Ko, D., Thangaraj, N., Marzan, D.E., and Swerdlow, N.R. (2009). Evaluating the antipsychotic profile of the preferential PDE10A inhibitor, papaverine. *Psychopharmacology (Berl)* 203, 723–735. <https://doi.org/10.1007/s00213-008-1419-x>.
  33. Benz, P.M., Laban, H., Zink, J., Günther, L., Walter, U., Gambaryan, S., and Dib, K. (2016). Vasodilator-Stimulated Phosphoprotein (VASP)-dependent and -independent pathways regulate thrombin-induced activation of Rap1b in platelets. *Cell Commun. Signal.* 14, 21. <https://doi.org/10.1186/s12964-016-0144-z>.
  34. Otopalova, E., Smith, S., Cheng, G., and Thannickal, V.J. (2020). Oxidative stress in pulmonary fibrosis. *Compr. Physiol.* 10, 509–547. <https://doi.org/10.1002/cphy.c190017>.
  35. Heukels, P., Moor, C.C., von der Thüsen, J.H., Wijsenbeek, M.S., and Kool, M. (2019). Inflammation and immunity in IPF pathogenesis and treatment. *Respir. Med.* 147, 79–91. <https://doi.org/10.1016/j.rmed.2018.12.015>.
  36. Ballester, B., Milara, J., and Cortijo, J. (2020). Pirfenidone anti-fibrotic effects are partially mediated by the inhibition of MUC1 bioactivation. *Oncotarget* 11, 1306–1320. <https://doi.org/10.18632/oncotarget.27526>.
  37. Sottirai, V.S., Sue, S.L., Batson, R.C., Frey, D.J., and Khaw, H. (1985). Effects of papaverine on smooth muscle cell morphology and vein graft preparation. *J. Vasc. Surg.* 2, 834–842. <https://doi.org/10.1067/mva.1985.av0020834>.
  38. Siuciak, J.A., Chapin, D.S., Harms, J.F., Lebel, L.A., McCarthy, S.A., Chambers, L., Shrikhande, A., Wong, S., Menniti, F.S., and Schmidt, C.J. (2006). Inhibition of the striatum-enriched phosphodiesterase PDE10A: a novel approach to the treatment of psychosis. *Neuropharmacology* 51, 386–396. <https://doi.org/10.1016/j.neuropharm.2006.04.013>.
  39. Verhoest, P.R., Chapin, D.S., Corman, M., Fonseca, K., Harms, J.F., Hou, X., Marr, E.S., Menniti, F.S., Nelson, F., O'Connor, R., et al. (2009). Discovery of a novel class of phosphodiesterase 10A inhibitors and identification of clinical candidate 2-[4-(1-methyl-4-pyridin-4-yl-1H-pyrazol-3-yl)-phenoxy]methyl]-quinoline (PF-2545920) for the treatment of schizophrenia. *J. Med. Chem.* 52, 5188–5196. <https://doi.org/10.1021/jm900521k>.
  40. Funke, U., Deuther-Conrad, W., Schwan, G., Maisonia, A., Scheunemann, M., Fischer, S., Hiller, A., Briel, D., and Brust, P. (2012). Radiosynthesis and radiotracer properties of a 7-(2-[18F]Fluoroethoxy)-6-methoxyppyrolidinylquinazoline for imaging of phosphodiesterase 10A with PET. *Pharmaceuticals* 5, 169–188. <https://doi.org/10.3390/ph5020169>.
  41. Hennenberg, M., Trebicka, J., Fischer, H.P., Heller, J., and Sauerbruch, T. (2009). Hepatic VASP upregulation in rats with secondary biliary cirrhosis by expression in the peribiliary vascular plexus. *Microvasc. Res.* 78, 235–240. <https://doi.org/10.1016/j.mvr.2009.05.002>.
  42. Piazza, G.A., Ward, A., Chen, X., Maxuitenko, Y., Coley, A., Aboelella, N.S., Buchsbaum, D.J., Boyd, M.R., Keeton, A.B., and Zhou, G. (2020). PDE5 and PDE10 inhibition activates cGMP/PKG signaling to block Wnt/ $\beta$ -catenin transcription, cancer cell growth, and tumor immunity. *Drug Discov. Today* 25, 1521–1527. <https://doi.org/10.1016/j.drudis.2020.06.008>.
  43. Li, N., Lee, K., Xi, Y., Zhu, B., Gary, B.D., Ramírez-Alcántara, V., Gurpinar, E., Canzoneri, J.C., Fajardo, A., Sigler, S., et al. (2015). Phosphodiesterase 10A: a novel target for selective inhibition of colon tumor cell growth, and  $\beta$ -catenin-dependent TCF transcriptional activity. *Oncogene* 34, 1499–1509. <https://doi.org/10.1038/onc.2014.94>.
  44. Chilosi, M., Poletti, V., Zamò, A., Lestani, M., Montagna, L., Piccoli, P., Pedron, S., Bertaso, M., Scarpa, A., Murer, B., et al. (2003). Aberrant Wnt/ $\beta$ -catenin pathway activation in idiopathic pulmonary fibrosis. *Am. J. Pathol.* 162, 1495–1502. [https://doi.org/10.1016/s0002-9440\(10\)64282-4](https://doi.org/10.1016/s0002-9440(10)64282-4).
  45. Hasaneen, N.A., Cao, J., Pulkoski-Gross, A., Zucker, S., and Foda, H.D. (2016). Extracellular Matrix Metalloproteinase Inducer (EMMPRN) promotes lung fibroblast proliferation, survival and differentiation to myofibroblasts. *Respir. Res.* 17, 17. <https://doi.org/10.1186/s12931-016-0334-7>.
  46. Gkretsi, V., Stylianou, A., and Stylianopoulos, T. (2017). Vasodilator-Stimulated Phosphoprotein (VASP) depletion from breast cancer MDA-MB-231 cells inhibits tumor spheroid invasion through downregulation of Migfilin,  $\beta$ -catenin and urokinase-plasminogen activator (uPA). *Exp. Cell Res.* 352, 281–292. <https://doi.org/10.1016/j.yexcr.2017.02.019>.
  47. Najafov, A., Seker, T., Even, I., Hoxhaj, G., Selvi, O., Ozel, D.E., Koman, A., and Birgül-Iyison, N. (2012). MENA is a transcriptional target of the Wnt/ $\beta$ -catenin pathway. *PLoS One* 7, e37013. <https://doi.org/10.1371/journal.pone.0037013>.
  48. Chen, S., Zhang, Y., Lighthouse, J.K., Mickelsen, D.M., Wu, J., Yao, P., Small, E.M., and Yan, C. (2020). A novel role of cyclic nucleotide phosphodiesterase 10A in pathological cardiac remodeling and dysfunction. *Circulation* 141, 217–233. <https://doi.org/10.1161/CIRCULATIONAHA.119.042178>.
  49. Weber, M., Breier, M., Ko, D., Thangaraj, N., Marzan, D.E., and Swerdlow, N.R. (2009). Evaluating the antipsychotic profile of the preferential PDE10A inhibitor, papaverine. *Psychopharmacology* 203, 723–735. <https://doi.org/10.1007/s00213-008-1419-x>.
  50. Wu, Q., Zhou, Y., and Zhou, X.M. (2019). Citrus alkaline extract delayed the

- progression of pulmonary fibrosis by inhibiting p38/NF- $\kappa$ B signaling pathway-induced cell apoptosis. *Evid. base Compl. Alternative Med.* 2019, 1528586. <https://doi.org/10.1155/2019/1528586>.
51. Joshi, N., Watanabe, S., Verma, R., Jablonski, R.P., Chen, C.I., Cheres, P., Markov, N.S., Reyfman, P.A., McQuattie-Pimentel, A.C., Sichizya, L., et al. (2020). A spatially restricted fibrotic niche in pulmonary fibrosis is sustained by M-CSF/M-CSFR signalling in monocyte-derived alveolar macrophages. *Eur. Respir. J.* 55, 1900646. <https://doi.org/10.1183/13993003.00646-2019>.
52. Frankel, S.K., Cosgrove, G.P., Cha, S.I., Cool, C.D., Wynes, M.W., Edelman, B.L., Brown, K.K., and Riches, D.W.H. (2006). TNF-alpha sensitizes normal and fibrotic human lung fibroblasts to Fas-induced apoptosis. *Am. J. Respir. Cell Mol. Biol.* 34, 293–304. <https://doi.org/10.1165/rcmb.2005-0155OC>.
53. Ashcroft, T., Simpson, J.M., and Timbrell, V. (1988). Simple method of estimating severity of pulmonary fibrosis on a numerical scale. *J. Clin. Pathol.* 41, 467–470. <https://doi.org/10.1136/jcp.41.4.467>.
54. Hubner, R.H., Gitter, W., El Mokhtari, N.E., Mathiak, M., Both, M., Bolte, H., Freitag-Wolf, S., and Bewig, B. (2008). Standardized quantification of pulmonary fibrosis in histological samples. *Biotechniques* 44, 507–511–514–517. <https://doi.org/10.2144/000112729>.

## STAR★METHODS

### KEY RESOURCES TABLE

REAGENT or RESOURCE	SOURCE	IDENTIFIER
<b>Antibodies</b>		
Rabbit Anti-Fibronectin	Genetex	CAT# GTX112794;RRID:AB_1950298
Rabbit Anti-Collagen I	Genetex	CAT# GTX20292; RRID:AB_384293
Rabbit Anti- $\alpha$ -SMA	Abcam	CAT# ab5694; RRID:AB_2223021
Rabbit Anti-b-catenin	Cell Signaling Technology	CAT# 8480; RRID:AB_11127855
Mouse Anti-VASP(A-11)	Santa Cruz	CAT# sc-46668; RID:AB_2213431
Rabbit Anti-VASP	Cell Signaling Technology	CAT# 3132; RRID:AB_2213393
Rabbit Anti-PDE10A	Abcam	CAT# ab14622; RRID:AB_301390
Rabbit Anti-P-VASP-157	Cell Signaling Technology	CAT# 3111; RRID:AB_331569
Rabbit Anti-P-VASP-239	Cell Signaling Technology	CAT# 3114; RRID:AB_2213396
Rabbit Anti-b-tubulin	Diagbio	CAT# db3285
Rabbit Anti-GAPDH	Genetex	CAT# GTX100118;RRID:AB_1080976
Rabbit Anti-Lamin B1	Diagbio	CAT# db35
Rabbit Anti-Lamin B1	Diagbio	CAT# db2396
Rabbit Anti-His	Diagbio	CAT# db2396
Goat Anti-IRDye680CW	LI-COR Biosciences	CAT# 926-32220; RID:AB_621840
Goat Anti-IRDye800CW	LI-COR Biosciences	CAT# 926-32211; RID:AB_621843
<b>Biological samples</b>		
Lung tissue	Isolated from C57 mice	N/A
Human Lung Fibroblasts	Isolated from clinical lung cancer patient	N/A
<b>Chemicals, peptides, and recombinant proteins</b>		
MTT	MTT	CAT# 1334GR001
TRlzol	Takara	CAT# 9109
Lipo2000	Invitrogen	CAT# 11668-019
HiScript II Q RT SuperMix for qPCR	Vazyme	CAT# R222-01
F12K Medium	Boster	CAT# PYG0093
DMEM/H Medium	Corning	CAT# 10-013-CVR
Opti-MEM Medium	Gibco	CAT# 31985-062
Phosphate Buffered Saline (PBS)	Solarbio	CAT# P1010
FBS	Corning	CAT# 35-081-CV
Protease Inhibitor Cocktail	Roche	CAT# 4693132001
Phosphatase Inhibitor Cocktail	Roche	CAT# 4906845001
Penicillin/Streptomycin	KeYi	CAT# CP011
TGFB1	Peprotech	CAT# 100-21
Trypsin	KeYi	CAT# CY003
DMSO	Sigma Aldrich	CAT# D5879
RIPA Lysis	Boster	CAT# AR0105
TRIS	Amresco	CAT# VWRB85827
SDS	Biofroxx	CAT# 3250KG001
Tris-HCl pH 8.8	Boster	CAT# AR1162

(Continued on next page)

**Continued**

REAGENT or RESOURCE	SOURCE	IDENTIFIER
Tris-HCl pH 6.8	Boster	CAT# AR1163
Tween 20	Sigma Aldrich	CAT# 93773
Papaverine (PAP)	Meilunbio	CAT# 93773
Pirfenidone (PFD)	Meilunbio	CAT# 61-25-6
ICG-001	MCE	CAT# HY-14428
Pf-2545920	Meilunbio	CAT# MB7418
Bleomycin (BLM)	Nippon Kayo	CAT# 600700
Amiodarone (AD)	Sanofi	CAT# 7A015
Protein A/G Magnetic beads	Med Chem Express	CAT# HY-K0202

**Critical commercial assays**

cAMP Parameter Assay Kit	R&D Systems	CAT# SKGE002B
cGMP Parameter Assay Kit	R&D Systems	CAT# KGE003
Sircol Soluble Collagen Assay	Bicolor	CAT# S1000
Nuclear and Cytoplasmic Protein Extraction Kit	Beyotime Biotechnology.	CAT# P0028
MDA Assay Kit	NanJing JianCheng	CAT# A003-1
SOD Assay Kit	NanJing JianCheng	CAT# A001-1
H&E Staining kit	NanJing JianCheng	CAT# D006
Masson Staining kit	NanJing JianCheng	CAT# D026
Bio-Rad Protein Assay Dye Reagent kit	Bio-Rad	CAT# 5000002
SYBR® green qPCR kit	Roche	CAT# 0488735200

**Deposited data**

RNA seq	<a href="http://nupulmonary.org/resources/">nupulmonary.org/resources/</a>	GSE122960
RNA seq	<a href="http://nupulmonary.org/resources/">nupulmonary.org/resources/</a>	GSE104154

**Experimental models: Cell lines**

HFL-1	ATCC	CAT# CCL-153
MRC-5	Cell Bank of Shanghai Academy of Sciences	CAT# CCL-171

**Experimental models: Organisms/strains**

C57BL/6 mice, 8 weeks old, adult male	SHANGHAI SLAC LABORATORY ANIMAL CO. LTD	N/A
---------------------------------------	---	-----

**Oligonucleotides**

Primers for RT-PCR analysis, see <a href="#">Table 1</a>	Sangon Biotech (Primers designed by BLAST)	N/A
VASP si-RNA sequence: 5'-GGACCUACAGAGGGUGAAAdTdT-3'	GenePharma	N/A

**Recombinant DNA**

pADM-PDE10A	Vigenebio	NCBI: NM_006661
-------------	-----------	-----------------

**Software and algorithms**

GraphPad Prism 7.01	Graphpad Software	<a href="https://www.graphpad.com">https://www.graphpad.com</a>
ImageJ software	NHI	<a href="https://imagej.net/software/imagej2/">https://imagej.net/software/imagej2/</a>
UCSC cell browser	UCSC cell browser	<a href="https://cells.ucsc.edu/">https://cells.ucsc.edu/</a>

## RESOURCE AVAILABILITY

### Lead contact

Further information and requests for resources and reagents should be directed to and will be fulfilled by the lead contact, Huifang Tang ([tanghuifang@zju.edu.cn](mailto:tanghuifang@zju.edu.cn)).

### Materials availability

All reagents were purchased commercially. This study did not generate new unique reagents.

### Data and code availability

All data reported in this paper will be shared by the [lead contact](#) upon request.

This paper does not report original code.

Any additional information required to reanalyze the data reported in this paper is available from the [lead contact](#) upon request.

## EXPERIMENTAL MODEL AND SUBJECT DETAILS

### Animals

Adult male 7-8-week-old C57BL/6N mice weighing 23–25 g were obtained from the Model Animal Research Center of Nanjing University. The animals were housed in an SPF-grade animal facility at  $23 \pm 2^\circ\text{C}$  and  $50 \pm 10\%$  humidity, with a simultaneous 12-h light and 12-h dark cycle. All animal care and handling procedures were approved by the Institutional Animal Care and Use Committee of Zhejiang University.

### Bleomycin induced lung fibrosis model

The control mice ( $n = 5$ ) was injected intratracheally with 20  $\mu\text{l}$  of sterile saline. Other mice were injected intratracheally with bleomycin at a dose of 4 U/kg, dissolved in 20  $\mu\text{l}$  of sterile saline. To study the effect of papaverine and pirfenidone, mice were injected intraperitoneally with papaverine (PAP) (4 mg/kg) or pirfenidone (PFD) (100 mg/kg) daily from day 7 to day 21. The dose of drugs used in this animal experiment was based on previous literature.<sup>49,50</sup> Mice were sacrificed by euthanasia on day 21, and lung tissues were collected for further analysis while body weight changes were recorded.

### Amiodarone induced lung fibrosis model

C57BL/6 mice were intratracheal injected with 20  $\mu\text{l}$  of 5% glucose (C,  $n = 5$ ) or amiodarone (6.25 mg/kg AD,  $n = 15$ ) at day 1, 3 and 5, respectively. To study the effect of papaverine and pirfenidone, mice were injected intraperitoneally with papaverine (PAP) (3 mg/kg) or pirfenidone (PFD) (100 mg/kg) ( $n = 5$ ) daily from day 7, and continuous administrated for 7 days. Mice were weighted every day and sacrificed 15 days after the first administration.

## METHOD DETAILS

### PDE10A gene expression validation in public data source

Single-cell RNA sequencing data from patients with pulmonary fibrosis from GSE122960<sup>23</sup> and mice exposed to bleomycin from GSE104154.<sup>24</sup> Based on UCSC cell browser (<https://cells.ucsc.edu/>), we used this dataset to reanalyze the PDE10A expressed cell cluster in the three single-cell RNA-Seq.<sup>23,24,51</sup>

- (1). Single-cell RNA-Seq was performed on single-cell suspensions generated from 8 lung biopsies from transplant donors and 8 lung explants from transplant recipients with pulmonary fibrosis. Cells were clustered using a graph-based shared nearest neighbor clustering approach and visualized using a t-distributed Stochastic Neighbor Embedding (tSNE) plot. See <https://doi.org/10.1164/rccm.201712-2410OC> for details.
- (2). Single-cell RNA-Seq generated from 3 normal mouse lungs and 3 fibrotic mouse lungs from Xie et al.<sup>28</sup> All samples were reanalyzed by Joshi et al,<sup>51</sup> and uploaded in UCSC cell browser. See <https://doi.org/10.1183/13993003.00646-2019> for details.

### Cell culture and treatment

Human fetal lung fibroblasts (HFL-1) cell line were cultured in Ham's F12K medium. After reaching confluence, the serum content of the medium was reduced to 0.4% FBS for starvation for 24 h. The cells were then stimulated with 10 ng/ml TGF $\beta$ 1 with or without papaverine for 48 h. The cells were used between passages 6-12.

MRC5 were cultured in DMEM/H medium. After reaching confluence, the serum content of the medium was reduced to 0.4% FBS for starvation for 24 h. The cells were then stimulated with 10 ng/ml TGF $\beta$ 1 with or without papaverine for 48 h. The cells were used between passages 6-12.

Primary human lung fibroblast (LFs) was obtained from the lung section of patients with lung cancer in second hospital of the Zhejiang University school of medicine. The specific experimental procedures refer to the literature.<sup>52</sup> LFs were used between passages 3-6 with DMEM/H medium.

### Adenovirus cell transfection

Adenovirus encoding human PDE10A (NM\_006661) was constructed by pADM-FH-GFP plasmid. It was named by pADM-PDE10A and C-terminus of the gene content a His tag, the viral titer was  $6.5 \times 10^{10}$  pfu/ml. Fibroblasts were plated on 6 cm dish. After 24 h, adenovirus of pADM-PDE10A was transfected into HFL-1 cells of MOI (multiplicity of infection) at 20 and 10 for 12 h. HFL-1 cells were then cultured for another 48 h for WB assay.

### Immunofluorescence

Fibroblasts were plated on 24-well chamber slides in culture medium until 70% confluent and then starved with 0.5% FBS for 24 h followed by combining with papaverine or pirfenidone. After 48 h, cells were fixed in 4% paraformaldehyde for 15 min and permeabilized in 0.5% Triton X-100 for 20 min. Cells were then blocked in 3% normal goat serum for 1 hour at room temperature, followed by incubation with  $\alpha$ -SMA primary antibody at 1:100 dilution in blocking solution for 12 h at 4 °C. Alexa 488-conjugated goat anti-rabbit antibody was used as secondary antibody and nuclei were stained using 4',6-diamidino-2-phenylindole (DAPI). The images were captured using fluorescence microscope. About fluorescence intensity quantification methods, we used software of Image J to quantification and every slide was pictured for 5 (20 $\times$ ) fields.

### The cAMP and cGMP measurement

The quantitative determination of cAMP and cGMP was performed using the assay kit. All process followed the instruction. Firstly, the primary antibody solution was added to all wells except the non-specific binding wells. After incubating for 1 hour at RT on horizon orbital microplate shaker, we then aspirate each well and wash for four times with wash buffer. After the last wash, the 50  $\mu$ l of cAMP conjugate was added to all wells as well as the 100  $\mu$ l standard, control or sample within 15 minutes on addition of the cAMP conjugate. The plate was replaced on the shaker for incubating for 2 hours at room temperature. Then repeating the wash steps as before, we add 200  $\mu$ l of substrate solution to each well to incubate for another 30 minutes at room temperature (avoid light). Lastly, the 100  $\mu$ l stop solution was added to each well, and the optical density was determined using microplate reader set to 450 nm within 30 minutes. The concentration of cAMP can be calculated corresponding the mean absorbance from the standard curve.

### Histological assessment of lung fibrosis model

Lung tissues were conventional fixed, dehydrated, embedded in paraffin. Slices with 4  $\mu$ m were prepared, following conventional deparaffinization and rehydration. The slices were stained with Hematoxylin-eosin or Masson trichrome staining according the protocol. blinded semi-quantitative scoring were performed using a modified Ashcroft score.<sup>53,54</sup> The criteria used in determining scores are outlined below: 0, Normal lung; 1, Minima fibrous thickening of alveolar or bronchiolar walls; 3, Moderate thickening of walls without obvious damage to lung architecture; 5, Increased fibrosis with definite damage to lung structure and formation of fibrous bands or small fibrous masses; 7, Severe distortion of structure and large fibrous areas; "honeycomb lung" is placed in this category; 8, Total fibrous obliteration of the field. As the criteria for grading lung fibrosis, in every field the predominant degree of fibrosis was recorded-that occupying more than half of the field area. The whole area of the circular microscope image was considered and the observer first decided whether the parenchyma in the field was normal or fibrotic. If normal tissue

predominated the field that was allotted a score of 0. If fibrotic tissue predominated the observer decided on the predominant level of fibrosis in the field, trying to place the field in one of the odd numbered categories. If there was any difficulty in deciding between two odd numbered categories the field would be given the intervening even numbered score. Fields predominantly occupied by portions of large bronchi or vessels, or by malignant tumor deposits, were not counted, and fields partly occupied by such structures were assessed on the predominant fibrosis in the remaining field area. Fibrosis alone was considered when arriving at a score and other changes which might be present, such as emphysema, were ignored. Cellular inflammatory exudate in airspaces was ignored but organized exudate was treated as fibrosis.

Alveolar septal thickness in AD model was quantified using ImageJ software,<sup>27</sup> The median was selected as the average value of selected images. By averaging different positions in each slide, the average value of each group of treatments is finally calculated.

### Soluble collagen assay

The total lung collagen content was assessed using the Sircol Soluble Collagen Assay by following the manufacturer's instructions. Briefly, lung tissue was diced and washed in cold phosphate buffered saline, then prepared homogenate using 200  $\mu$ l acid-pepsin extraction buffer and incubated at 4°C overnight for releasing the collagen. After centrifuged at 12,000 rpm for 10 min, supernatants (20  $\mu$ l) were collected and diluted five times in lysis buffer, added to 1 ml of Sircol Dye Reagent and then mixed in a gentle mechanical shaker for 30 min. The collagen-dye complex was precipitated by centrifugation at 12,000 rpm for 10 min and the unbound dye solution was then carefully removed by washing with 750  $\mu$ l ice-cold Acid-Salt Wash Reagent. The precipitated complex was dissolved by adding 250  $\mu$ l Alkali Reagent. The absorbance of 200  $\mu$ l of sample supernatant was read at 555 nm and plotted a standard curve with series known concentration standards. Absolute collagen content was calculated by comparing sample values to a standard curve.

### Oxidative stress indexes

Lobes of lungs (except lower lobes of right lungs) were homogenized with PBS solution (1 ml/100 mg), and the homogenate was centrifuged at 3000 rpm for 10 minutes at 4 °C. Then the supernatant was collected, using the MDA and SOD assay kits to analyze the corresponding oxidative stress indexes. The malondialdehyde (MDA) measurement in the lung tissues is based on the reaction of MDA with thiobarbituric acid (TBA), who form a complex with maximum absorbance at 532 nm. The superoxide dismutase (SOD) measurement in the lung tissues is based on the reaction of SOD with xanthine/xanthine oxidase system, who form  $O_2^-$  oxidating hydroxylamine to nitrite. Nitrite has maximum absorbance at 550 nm.

### RNA isolation and RT-qPCR

The total RNA was extracted from lung tissue or cells by TRIzol<sup>TM</sup> reagent. cDNA synthesis was performed by using HiScript<sup>®</sup> II Supermix with 1  $\mu$ g of total RNA. Real-time qPCR was used to quantify the mRNA level of the gene using a SYBR green qPCR kit in 480 II qPCR system. GAPDH or  $\beta$ -actin was used as an internal standard. Primers were synthesized by Sangon Biotech (Sangon Biotech, Shanghai, China). Primers information was summarized in Table 1. After cDNA amplification, the relative gene expression was calculated using the  $2^{-\Delta\Delta Ct}$  method.

### $\beta$ -catenin nuclear translocation

Whole protein extracts were prepared from cells treated with drugs, resolved by EDTA solution. Cells were collected after 1,000 rpm, 5 min, followed by nuclear and cytoplasmic protein extraction kit to analyze the  $\beta$ -catenin protein expression.

### Immunoprecipitation (IP) assay

Cells were collected, lysed using western and IP lysis buffer supplemented with protease inhibitor cocktail for 30 min on ice, and centrifuged at 12,000  $\times$  g for 15 min. After protein quantification using a Bio-Rad Protein Assay Dye Reagent kit, clarified lysates were incubated with anti-VASP mouse antibody (10  $\mu$ g/ml) overnight at 4°C and magnetic protein A/G beads for 4 hat 4°C. Normal mouse immunoglobulin (IgG) was used as a negative IP control. The beads were washed at least five times with western and IP lysis buffer, and proteins were eluted by boiling in 1  $\times$  loading buffer at 100°C for 5 min and then used for western blotting.



### Western blot analysis

Whole protein extracts were prepared from lungs or cells. After homogenized in cold RIPA buffer containing 1×PhosSTOP, 1% protease inhibitor cocktail and 2% PMSF for 30 min, 30 μg of total protein from lung homogenate or cells were separated by SDS-PAGE. After membranes transferring and blocked with blocking buffer, proteins then incubated with primary antibodies overnight at 4°C. The membranes were subsequently incubated with secondary antibody (IRDye 800CW Goat Anti-Rabbit IgG; IRDye 800CW Goat Anti-Mouse IgG) and imaged with LI-COR's Odyssey Infrared Imaged System. Quantification analysis were performed by using Image J software.

### QUANTIFICATION AND STATISTICAL ANALYSIS

Prism 7.0 was used for statistical analysis. Data were presented as means ± SEM. All experiments were performed in triplicate in at least three independent trials. Data were analyzed with one-way ANOVA and Student's t-test where appropriate.  $p < 0.05$  was considered statistical differences.